# Impact of the extinction behaviour of sic lattices on their conductive-radiative heat transfers

Benoit Rousseau, Salih Ouchtout, Laurent Cangémi, Yann Favennec, Jérôme Vicente, Franck Enguehard

# IMPACT OF THE EXTINCTION BEHAVIOUR OF SIC LATTICES ON THEIR CONDUCTIVE-RADIATIVE HEAT TRANSFERS

**B. Rousseau[1], S. Ouchtout[2], L. Cangémi[2], Y. Favennec[1], J. Vicente[3], F. Enguehard[4]**

[1]Nantes Université, CNRS, LTeN, Nantes, 44306, France
[2]IFP Energies Nouvelles, 92852, Rueil-Malmaison
[3]Aix Marseille University, CNRS, IUSTI, Marseille, 13453, France
[4]Université de Poitiers, ISAE-ENSMA, CNRS, Institut P', Futuroscope Chasseneuil, 86360, France

## ABSTRACT

Refractory architected ceramics constitute a class of highly porous media which gains in importance for enginnering high-temperatures applications. From a thermal modelling viewpoint, one of the main challenges, is to finely describe the transport of thermal radiation which plays a major role in the dtermination of their thermal performances. Such a consideration is today crucial for developing topology optimization processes in order to define the best 3D geometries for a given set of objectives. To conduct these methodologies, it is important to quickly solve the radiative transfer equation at the continuous scale while taking into account as accurately as possible the meso-texture desbribing the 3D solid network. This goes back to assume that the physical statements governing this equation are valid, the porous architectures having to behave as an equivalent Beerian medium. However, when non Beerian behaviour is highlighted, the latter framework needs to be revised. To go one step further with this issue, numerical 3D geometries with a regular arrangement of cubic cells are generated with an homemade software. The analysis of their extinction cumulative distribution function curves obtained with the Radiative Distribution Function Identification method allows us to check whether or not the attenuated thermal radiation follows a Beerian behaviour. The effects of the textural parameters will then be discussed. Finally, preliminary practical considerations will be given for describing their conductive radiative behaviour when they are enclosed between a hot and a cold plate through both a continuous and the discrete scale methodologies, using a stabilized vectorial Finite Element Method solver.

**KEY WORDS:** Cellular lattices, Radiative Distribution Function Identification, non Beerian behaviour, conduction-radiation coupling.

## 1. INTRODUCTION

In the field of carbon-free heat generation, there is a growing interest in the design of compact and long-life high temperature energy systems such as gas-to-gas heat exchangers [1], volumetric solar receivers [2] (VSR) and radiant tube inserts [3], among others. They are mostly based on architected refractory ceramics (p ~75-95%, cell size ~0.1-10 mm) which can be depicted by a continuous ligament network (the solid phase) delimiting open cells in which a fluid can flow. When silicon carbide (SiC) is used as the constitituve material [2, 4], the whole 3D architecture exhibits outstanding properties such as high specific surface area, good flow-mixing capacity, high thermal shock resistance and high resistance to chemical corrosion. The rapid development of additive manufacturing (AM) extends furthermore the possibilities to elaborate a large range of 3D geometries going from regular lattice structures with different types of unit cells, triply periodic minimal surface-based structures up to more classical irregular strut-based structures. In order to propose a topology optimization process aiming at the definition of the best 3D architectures for prescribed thermal objectives, the detailed modelling of their thermal behaviour is essential [3, 5]. In particular, one of the main challenges, is to be able to exactly describe the role of thermal and/or solar radiation in the heat balance of the system for both unsteady or steady regimes. To date, two main routes can be used to determine the temperature and/or heat flux fields within 3D structures [5-8]. The first class of methods, at the discrete mesoscopic scale, allows a

*Corresponding Author : benoit.rousseau@univ-nantes.fr

treatment of the radiative heat exchange directly at the scale of the individual constituents (here the struts and walls constituting the basic cells). Several parallelized approaches have been developed for conducting these approaches : stabilized vectorial Finite Element schemes [5], cell centered Finite Volume models with ray tracing [9, 10], hybrid schemes combining motion of Brownian walkers in the solid opaque phase and ray tracing in the fluid phase [11], and Monte Carlo strategies based on integral formulations [12]. The second class of method, at the continuous macroscopic scale, requires to rigorously solve the radiative transfer equation as long as the assumptions (randomness, homogeneity and continuity) that govern its statement are valid. Let us clarify that an architected ceramic can be viewed as an equivalent domain absorbing, emitting and scattering the thermal radiation. These latter physical phenomena are, in fact, induced by the light-matter interaction at the scale of the ligaments. If the equivalent medium is optically thick, the radiative transfer equation can be reduced to a simpler diffusion equation by applying, for example, the spherical harmonics method at the order 1 (the P1 approximation) or, even more crudely, the Rosseland approximation [6]. Whatever the precision sought, these approaches can only be applied if the volume radiative properties (extinction, absorption and scattering coefficients, scattering phase function) are identified from an equivalent semitransparent continuous Beerian medium. The term Beerian stands, here, for an extinction law characterised by an exponential function of the optical thickness. This statement changes when spatial correlations occur meaning that the equivalent semitransparent medium becomes not easily homogeneisable. In general, the samples are considered as Beerian media [3, 13, 14] without an in-depth investigation of their ability to extinct radiation being really carried out. By using the Radiative Distribution Function Identification method, Taine et al. have shown that a dispersion of overlapping transparent spheres in an opaque continuous hosting medium deviates from the Beerian behavior when its volume fraction, $f_v$, becomes important ($f_v$ > 0.4) [15]. Such a synthetic medium can be used to represent a statistically isotropic foam. More recently, Ouchtout et al. have computed the temperatures fields within two SiC-based regular cubic lattices ($p$ = 0.91, $d_{nom}$= 0.16 mm, $L$ = 0.38 and 0.76 mm) by solving a conductive-radiative numerical scheme with stabilized vectorial finite element methodologies applied respectively at both the continuous scale and the discrete scale. Both the temperature profiles are closely identical [5]. Since the continuous approach assumes for the radiative part that the Beer law is valid, it can be concluded that this cubic lattice exhibits a Beerian behaviour. Such a survey indicates that a study investigating the radiative behavior of synthetic lattices as a function of variable textural features (spatial repartition, shape and size of cells, size of the computing domain) is still relevant. To go one step further with these issues, a set of virtual regular SiC-based cubic cell structures with prescribed textural features will be designed with the GenMat software (C++, Qt) [16]. Then, the Radiative Distribution Function Identification method will be applied to compute the extinction cumulative distribution functions of the whole set of numerical samples. This will allow us to provide preliminary practical criteria for defining the radiative behaviours (non Beerian or Beerian) of the samples. A set of extinction coefficients will be determined and their impacts on the modelling of the conductive-radiative behaviour of the cubic cells structures will be discussed.

## 2. NUMERICAL METHODOLOGIES

### 2.1 3D structures generation

In this work, a homemade 3D structures generator, called GenMat (C++, Qt) [16], has been used to provide the whole set of numerical samples. The generator allows the numerical elaboration of regular and irregular 3D structures with prescribed textural features (porosity, nominal pore diameter). For the regular structures, a simplified four-steps process is applied. The centers of all cells are firstly created. Secondly, the nodes, edges, faces of all cells are defined, and a structuration loop adds solid voxels between each apex, forming a thin skeleton. Thirdly, as for irregular foams, the ligaments can be shaped with a spherical or a square structuring element. Lastly, the desired porosity is reached by creating a distance map converted in grey levels. Once the 3D binarized structures are generated, a robust marching cube process allows to mesh the fluid/solid interface. GenMat proposes an export module for recording surfacic meshes.The software also contains modules which provide the volume fraction of the void phase i.e. the porosity, $p$, and the volumetric surface, $A$ of each numerical sample.

## 2.2 Radiative Distribution Function Identification method

In this work, the Radiative Distribution Function Identification (RDFI) method, originally proposed by Tancrez and Taine [17], will be applied to determine the volumetric radiative properties of the 3D architectures. This method has been implemented in the GenMat framework [18]. More precisely, the RDFI is a collision-based Monte Carlo Ray Tracing method assuming that for each local interaction between a ray and the solid matter, the geometrical optic approximation is valid. It means that the mean characteristic size of the ligaments and of the cells constituting the generated 3D structures must be much larger than the incident wavelength i.e. the Mie size parameter is greater than 1. The RDFI method consists in launching a huge number of rays from points $M$ that are uniformly distributed in the fluid phase surrounding the ligaments. Their directions are randomly chosen within the entire $4\pi$ steradian sphere. Once a ray hits a solid phase element at the point $I$, the latter is considered as totally extinguished and the path length to collision, $s_e = |MI|$ is computed [17]. For a large number of rays, $N_R$, a set of path length $s_{e,j}$ values are obtained from which the corresponding normalized extinction distribution function, $F_e(s)$ is computed :

$$F_e(s) = \frac{1}{N_R}\sum_{j=1}^{N_R} \delta\left(s - s_{e,j}\right) \tag{4}$$

where $s$ is the path length variable and $\delta$ the Dirac delta distribution. The extinction cumulative distribution function $G_e(s)$ is then obtained by integrating $F_e(s)$ :

$$G_e(s) = \int_0^s F_e(s')ds' \tag{5}$$

To decide whether the extinguished ray is absorbed or scattered, a random number, $\eta$, uniformly distributed over [0,1] is selected and compared to the local reflectivity, $\rho$, that can be given by the Fresnel law (if the interacting fluid/solid interface is considered as optically smooth). If $\eta > \rho$ the ray is considered as absorbed and otherwise scattered. This allows to determine the absorption and the scattering cumulative probabilities with a similar numerical process as for $G_e(s)$. If the studied equivalent medium is Beerian, the quantity $\left(1 - G_e(s)\right)$ shows a typical Beer-Lambert exponential decay behaviour expressed by:

$$1 - G_e(s) = e^{-\beta s} = \frac{I(s)}{I_0} \tag{6}$$

where $I(s)$ is the radiant intensity at the distance $s$ and $I_0$ is the impinging intensity at $s$ = 0 from a collimated beam. In that situation, the extinction coefficient $\beta$ of the equivalent Beerian medium can be evaluated by a fit of the numerically evaluated $\left(1 - G_e(s)\right)$ function.

## 2.3 Models of conductive radiative transfers

Before describing the two approaches used in this work and described in [5], let us specify that the global computational domain is depicted by a cube sandwhiched, on two of its opposite faces, by a hot opaque wall maintened at $T^{hot}$ (for $x = x_{min}$) and a cold opaque wall (for $x = x_{max}$) with $T = T^{cold}$.

### 2.3.1 Continuous-scale coupled model

For the continuous-scaled coupled model, the standard steady-state form of the radiative transfer equation, which describes the transport of the radiative intensity, $I(\boldsymbol{x}, \boldsymbol{s})$, within a Beerian semi-transparent medium is used :

$$\boldsymbol{s}.\nabla I(\boldsymbol{x}, \boldsymbol{s}) + \beta(\boldsymbol{x}) I(\boldsymbol{x}, \boldsymbol{s}) - \sigma(\boldsymbol{x}) \int_{4\pi} I(\boldsymbol{x}, \boldsymbol{s}')\Phi(\boldsymbol{s}', \boldsymbol{s})d\boldsymbol{s}' - \kappa(\boldsymbol{x})\frac{1}{\pi}\sigma_B n^2 T^4 = 0 \tag{7}$$

Here, $\boldsymbol{x} = (x, y, z) \in \Omega$ where $\Omega$ is the spatial domain of interest, $\boldsymbol{s} \in S^2$ is the direction of propagation where S is the solid angle space, $\beta(\boldsymbol{x}) = \kappa(\boldsymbol{x}) + \sigma(\boldsymbol{x})$ is the extinction coefficient with $\kappa(\boldsymbol{x})$the absorption coefficient and $\sigma(\boldsymbol{x})$ the scattering coefficient, $\sigma_B$ is the Stefan-Boltzmann constant, $m$ is the real part of the complex index of refraction of the medium and $T$ the temperature. $\Phi(\boldsymbol{s}, \boldsymbol{s}')$ is the scattering phase function which is depicted in this work by the Henyey-Greenstein function. In the present study, the spatial domain of interest $\Omega$ is a cube i.e. $\Omega = \{(x, y, z) | x \in [0, L], y \in [0, L], z \in [0, L]\}$. To provide closure to the model, the following boundary conditions are used for inward directions $\boldsymbol{s}.\boldsymbol{n} < 0$:

$$I(\boldsymbol{x}, \boldsymbol{s}) = \varepsilon \frac{1}{\pi} \sigma_B n^2 T^4 \;\; \forall x = \{x_{min}, x_{max}\} \tag{8}$$

$$I(\boldsymbol{x}, \boldsymbol{s}) = (1 - \varepsilon) I(\boldsymbol{x}, \boldsymbol{s}') \;\; \forall x = ]x_{min}, x_{max}[ \tag{9}$$

where $\varepsilon$ is the total emissivity of the two emissive walls at $x_{min}$ (fixed at $T^{hot}$) and $x_{max}$ (fixed at $T^{cold}$). Furthemore $\boldsymbol{s}'$ is deduced from $\boldsymbol{s}$ by using the Householder rotation matrix. The Eq. (9) depicts periodic boundary conditions with specular reflection for the four other faces of the cube. The knowledge of $I(\boldsymbol{x}, \boldsymbol{s})$ allows to compute the integrated intensity $G(\boldsymbol{x})$ defined by :

$$G(\boldsymbol{x}) = \int_{4\pi} I(\boldsymbol{x}, \boldsymbol{s}) d\boldsymbol{s} \tag{10}$$

This latter quantity is injectetd in the steady-state heat energy balance which writes :

$$\nabla.(-\lambda(\boldsymbol{x})\nabla T) + \kappa(\boldsymbol{x}) 4\pi I_b(T) - \kappa(\boldsymbol{x}) G(\boldsymbol{x}) = 0 \tag{11}$$

with $I_b(T) = 1/\pi \, \sigma_B n^2 T^4$. The boundary conditions for solving Eq. (11) are the following :

$$T = T^{hot} \;\; \forall x = \{x_{min}\}, \; T = T^{cold} \;\; \forall x = \{x_{max}\}, -\nabla T.\boldsymbol{n} = 0 \;\; \forall x = ]x_{min}, x_{max}[ \tag{12}$$

2.3.2 Discrete-scale coupled model

The discrete-scale coupled model consists in considering a solid phase domain, $\Omega_s$, immersed in a fluid phase domain, $\Omega_f$. $\Omega_s \cup \Omega_f$ forms the whole computational domain $\Omega$. This description corresponds well to domains defined from the 3D architectures given by GenMat. The solid (resp. fluid) phase boundary is given by $\partial\Omega_s$ (resp. $\partial\Omega_f$) and the solid-fluid interface is denoted by $\Gamma = \partial\Omega_s \cap \partial\Omega_f$. Let us define $\boldsymbol{n_s}$ (resp. $\boldsymbol{n_f}$**)** the outward unit vector normal to the solid (resp. fluid) phase. The approach has already been detailed elsewhere [5, 19] and is now decribed briefly. First the steady-state heat conduction equation is solved in the solid phase which must be optically thick. The energy transfer between the solid phase and the void phase occurs at the boundary only. The conduction problem consists in searching a scalar function $T_s$ verifying :

$$\nabla.(-\lambda_s \nabla T_s) = 0 \;\; \forall x \in \Omega_s \tag{13}$$

where $\lambda_s$ is the thermal conductivity of the solid phase. Similarly to the continuous-scale model, the temperature is prescribed on the opposite parts of the solid phase.

$$T_s = T^{hot} \text{ on } \partial\Omega_{s,D,-} \subset \Gamma \text{ with } \partial\Omega_{s,D,-} = \{x \in \partial\Omega_s, \boldsymbol{x} < \delta + min_{\Omega^s} \boldsymbol{x}'\} \tag{14}$$

$$T_s = T^{cold} \text{ on } \partial\Omega_{s,D,+} \subset \Gamma \text{ with } \partial\Omega_{s,D,+} = \{x \in \partial\Omega_s, \boldsymbol{x} < \delta + max_{\Omega^s} \boldsymbol{x}'\} \tag{15}$$

In these relationships, the subscript $D$ stands for Dirichlet and $\delta$ is a sufficiently small positive parameter so that the Dirichlet condition is applied on a boundary of sufficiently large enough area. The boundary condition over Γ are flux continuity relations taking into account both the emission loss and the incoming flux radiation:

$$-\lambda_s \nabla T_s . \boldsymbol{n_s} = \varepsilon_s \sigma_B n_s^2 {T_s}^4 - \varepsilon_s \int_{s.\boldsymbol{n_f}>0} I_f \, \boldsymbol{s}.\boldsymbol{n_f} d\boldsymbol{s} \tag{16}$$

where $n_s$is the index of refraction of the solid phase and $T_s$ the temperature on Γ. Furthermore the radiation problem is only solved in the fluid phase (considered here as purely transparent) where the steady state radiative transfer equation is reduced to :

$$\boldsymbol{s}.\nabla I_f = 0 \ \ \forall x \in \Omega_f \tag{17}$$

Since thermal exchanges can occur on Γ, an inlet boundary condition is defined (the " ͡ " symbol stands for inlet condition):

$$\hat{I}(\boldsymbol{x},\boldsymbol{s}) = \varepsilon_s \frac{1}{\pi} \sigma_B n^2 T^4 + (1-\varepsilon_s)\, I(\boldsymbol{x},\boldsymbol{s}') \text{ on } \Gamma \text{ with } \boldsymbol{s}.\boldsymbol{n_f} < 0 \tag{18}$$

The problem is closed by considering on the two ends of $\Omega_f$, the two hot and cold prescribed temperatures, yielding the relationship:

$$I(\boldsymbol{x},\boldsymbol{s}) = \varepsilon \frac{1}{\pi} \sigma_B n^2 \left(T^{hot}\right)^4 \ \ \forall x = \{x_{min}\} \text{ and } I(\boldsymbol{x},\boldsymbol{s}) = \varepsilon \frac{1}{\pi} \sigma_B n^2 \left(T^{cold}\right)^4 \ \ \forall x = \{x_{max}\} \tag{19}$$

## 3. RESULTS AND DISCUSSION

In the following, the room-temperature complex refractive index of silicon carbide at the wavelength of 4 µm, is affected to the solid skeleton of each numerical 3D structure [21]. It ensures that their ligaments can be considered as optically thick, their lowest diameter being fixed at 30 µm. For the sake of clarity, the acronym CCS means cubic cell structures. To complete their denomination, one adds an information regarding the nominal pore diameter, $d_{nom}$, the number of cells, $N_c$, and the size of the domain, $L$. CCS_160_1_380 corresponds therefore to a cubic cell structure with $d_{nom}$ = 160 µm, $N_c$= 1 and $L$ = 380 µm.

### 3.1 Influence of the textural parameters of cubic cell structures on their extinction behaviour

Five cubic cell structures with a growing cell number ($N_c$= $1^3$, $3^3$, $5^3$, $7^3$, $9^3$) with same size ($d_{nom}$ = 160 µm) are firstly created with GenMat. Table 1 gives their respective porosity and volumetric surface after having performed the final porosity tuning process as explained in section 2.1. The numerical samples are described in Fig.1

**Table 1** Textural and radiative parameters

| Samples | $p$ | $L$ (µm) | $A$ ($m^{-1}$) | $\beta^{om}$($m^{-1}$) | $a$ | $b$ ($m^{-1}$) |
|---|---|---|---|---|---|---|
| CCS_160_1_380 | 0.91 | 380 | 8755.6 | 2405.4 | 1.53 | 4424.8 |
| CCS_160_27_760 | 0.91 | 760 | 8580.4 | 2357.1 | 3.57 | 1295.3 |
| CCS_160_125_1040 | 0.91 | 1040 | 8521.2 | 2341.0 | 6.21 | 642.7 |
| CCS_160_343_1330 | 0.91 | 1520 | 8698.0 | 2389.6 | 6.24 | 595.2 |
| CCS_160_729_1710 | 0.91 | 1900 | 8716.2 | 2394.6 | 10.58 | 351.5 |

The analysis of their two-point autocorrelation functions indicate that the influence of the lattice periodicity weakens when the size of the computational domain becomes important. Fig. 2) shows their extinction cumulative distribution functions $ln\left(1-G_e(s)\right)$ as a function of $s$, obtained for $N_R$ = $10^6$.

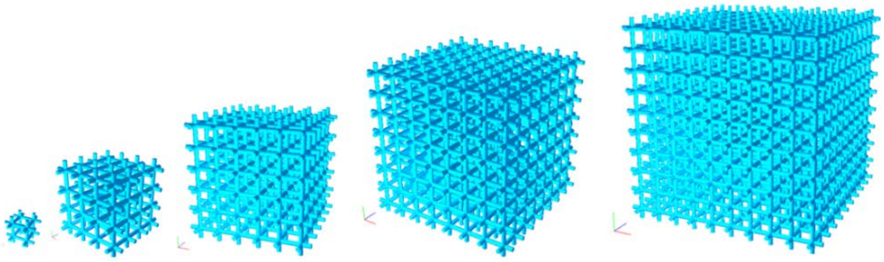

**Fig.1** 3D images of (1) CCS_160_1_380 (2) CCS_160_27_760, (3) CCS_160_125_1040 (4) CCS_160_343_1330 (5) CCS_160_729_1710

Special cares have been taken to define a suitable shooting zone for computing $ln\left(1 - G_e(s)\right)$ i.e., not too small to be representative, and not too large to limit outgoing rays. The curves clearly deviate from what is expected for a Beerian behaviour (a perfect linear profile is expected in this case). It is noted that the deviations are all the less proncunced when the size of the computational domain become large. To go one step further, each extinction cumulative distribution function curve has been nicely reproduced using the Levengberg-Marquardt scheme by the following expression:

$$y(s) = -a\left(e^{bs} - 1\right) \tag{20}$$

The results of the fitting process are shown for for CCS_160_1_380 and CCS_160_27_760 in Fig2b). In Gomez-Garcia et al, the authors proposed a quite similar expression for analysing the radiation propagation within a stack of SiC-based square grids [20]. Table 1 lists the values of $a$ and $b$ for the five numerical samples. Going from CCS_160_1_380 up to CCS_160_729_1710, it can be evidenced that the lowest value of $b$ are required to confer a Beerian behaviour to the set of numerical 3D architectures. It is worth of notify that if $bs$ is lower than 1, $y(s) \sim -abs$ and then the extinction curve becomes Beerian.

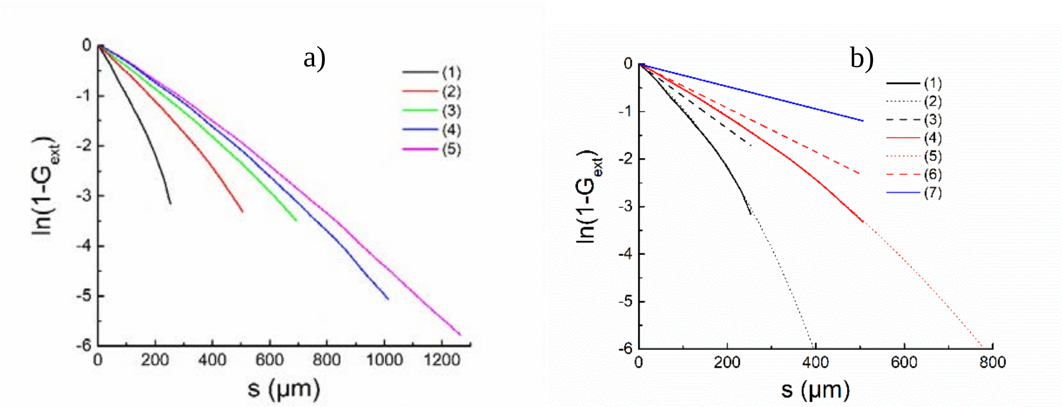


**Fig2 a)** Extinction cumulative distribution function: (1) CCS_160_1_380 (2) CCS_160_27_760, CCS_160_125_1040 (4) CCS_160_343_1330 (5) CCS_160_729_1710 **b)** (1) Extinction cumulative distribution function for CCS_160_1_380 (2) Fitted curve with Eq. 20 for CCS_160_1_380 (3) $-\beta^{as}s$ for CCS_160_1_380 (4) Extinction cumulative distribution function for CCS_160_27_760 (5) Fitted curve with Eq. 20 for CCS_160_27_760 (6) $-\beta^{as}s$ for CCS_160_27_760 (7) $-\beta^{om}s$ for CCS_160_27_760

By using Eq. (6) and Eq. (20), one can deduce the following relationship $\beta(s) = y(s)/s$. For small values of $s$, the exponential term can be approximated by its Taylor expansion and in this case, $\beta^{as} \sim ab$. Here, $\beta^{as}$ represents the asymptotic value of $\beta(s)$. This latter quantity is different from $\beta^{om} = A/4p$ which is the value of the extinction coefficient for a pure beerian medium at the optically thin limit. With GenMat, one can also check by fixing $L$, and by progressively increasing $d_{nom}$, that the deviation to the Beerian behaviour become more accentuated. On the other side, by keeping $N_c$ constant and decreasing $d_{nom}$ so that $L$ is homothetically reduced, the deviation to the Beerian behaviour appears more and more important. In conclusion, it can be highligted that for regular cubic cell architectures constituted of an opque solid network a large value of $L$ combined with a low value of $d_{nom}$ must exhibit an extinction feature closed to the one that can be expected from a Beerian medium.

## 3.2 Influence of the textural parameters of cubic cell structures on their conductive-radiative behaviour

In this last part, the different extinction coefficients reported in Table 1 for CCS_160_1_380 and CCS_160_27_760 are used when the continuous-scale (CS) coupled approach described in section 2.3. is applied. Let us recall that this work is focused on solid opaque phases (SiC-based consolidated networks) immersed within a transparent fluid phase. This suggests that their corresponding homogeneized extinction coefficients must be equal to those corresponding to their fluid phase (here $\beta(x)$ and $\beta^{as}$) as demonstrated Baillis et al. in Ref. [21] for metallic foams constituted of opaque skeletons immersed in air.

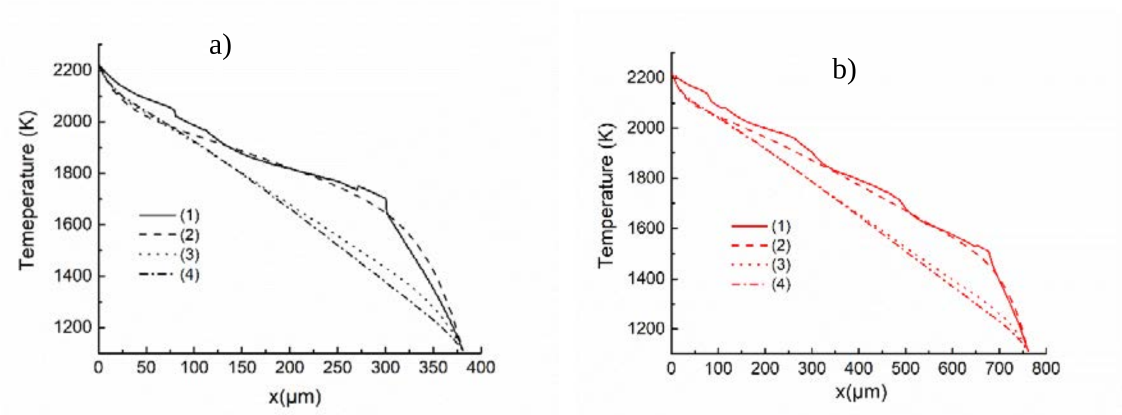


**Fig 3 a)** Average temperature along the axis of propagation with (1) the DM approach (2) the CS approach with $\beta^{om}$ (3) the CS approach with $\beta^{as}$ (4) the CS approach with $\beta(x)$ for CCS_160_1_380 **b)** Average temperature along the axis of propagation with (1) the DM approach (2) the CS approach with $\beta^{om}$ (3) the CS approach with $\beta^{as}$ (4) the CS approach with $\beta(x)$ for CCS_160_27_76

In addition to the CS approach, the discrete-scale (DM) coupled approach, also exposed in section 2.3, is directly used with the two 3D structures. Concerning the stabilized vectorial Finite Element Method framework required to solve the set of equations for the two approaches and the post-processing method developed for extracting the temperature profiles, full details are given in Ref [5, 19]. As previsouly evoked, we solve the conductive-raditive problem pionneringly defined by Grosh and Vistankta for a 1D geometry where a semi-transparent medium is sandwhiched between two isothermal parallel opaque plates with different temperatures ($T^{hot}$ = 2222 K and $T^{cold}$ = 1111 K) [22]. Let us explain that for the DM approach, $\varepsilon_s$ = 0.9 and $\lambda_s$= 30 W.m$^{-1}$.K$^{-1}$. In this work, the curves given by the DM method are considered as the reference data (see curves 1 in Fig. 3a and Fig. 3b). For the two numerical samples, the injection of $\beta^{om}$ in Eq. (7) gives temperature profiles pretty closed to those computed through the DM approach. However, when $\beta^{as}$ and $\beta(x)$ are used in the CS approach for CCS_160_1_380 and CCS_160_27_760, it can be emphasised that the temperature profiles present stronger differences. Indeed, the injection of $\beta^{as}$ and $\beta(x)$ in the Eq. (7) tends to increase the conduction-to-radiation parameter (i.e. the Planck number) which results in an unexpected conductive behaviour. The differences with the reference profiles ($\Delta T_{max}$ ~ 300 K in CCS_160_1_380) are the most important at more than three quarters of the propagation of the radiation in the two porous structures. Moreover, the use of $\beta(x)$ tends to accentuate the conductive transfer and to decrease the radiative one.

## 4. CONCLUSION

This work combines the numerical generation of cubic lattices constituted of SiC, the determination of their extinction cumulative distribution functions and the computation of the their conductive-radiative behaviour respectively with a FEM-based continuous-scale and a discrete scale approaches. All the numerical samples can be considered as non-Beerian and their extinction cumulative distribution functions can be described with an exponential growth law as a function of the variable path length. It can be underlined that the injection of the exctintion coefficient, obtained at the optically thin limit in the framework of the Radiative Distribution Function Identification method, in the continuous scale approach give results quite similar to what one can be directly computed on the 3D images through the discrete scale approach. For regular macroporous 3D architectures, more works are required to finely connect their extinction coefficients (and their possible spatial variation) for each considered phase (fluid and solid) with the exact corresponding effective extinction coefficient required to solve the radiative transfer equations at the macroscopic scale.

## REFERENCES


[1] Bayaniahangar R, Okoh I, Nawaz K, Cesarano J, Bigham S. Toward extreme high-temperature supercritical CO2 power cycles: Leakage characterization of ceramic 3D-printed heat exchangers. Additive Manufacturing. 2022;54:102783.
[2] Heisel C, Caliot C, Chartier T, Chupin S, David P, Rochais D. Digital design and 3D printing of innovative SiC architectures for high temperature volumetric solar receivers. Solar Energy Materials and Solar Cells. 2021;232:111336.
[3] Pelanconi M, Barbato M, Zavattoni S, Vignoles G, Ortona A. Thermal design, optimization and additive manufacturing of ceramic regular structures to maximize the radiative heat transfer. Materials & Design. 2019;163:107539.
[4] Pelanconi M, Zavattoni S, Cornolti L, Puragliesi R, Arrivabeni E, Ferrari L, et al. Application of ceramic lattice structures to design compact, high temperature heat exchangers: material and architecture selection. Materials. 2021;14:3225.
[5] Ouchtout S, Rousseau B, Favennec Y. Finite element framework for modeling conducto-radiative transfers within heterogeneous media at both discrete and continuous scales. International Journal of Heat and Mass Transfer. 2022;197:123274.
[6] Avila-Marin A, Fernandez-Reche J, Martinez-Tarifa A. Modelling strategies for porous structures as solar receivers in central receiver systems: A review. Renewable and Sustainable Energy Reviews. 2019;111:15-33.
[7] Petrasch J, Haussener S, Lipiński W. Discrete vs. continuum-scale simulation of radiative transfer in semitransparent two-phase media. Journal of Quantitative Spectroscopy and Radiative Transfer. 2011;112:1450-9.
[8] Xia X-L, Li Y, Sun C, Ai Q, Tan H-P. Integrated simulation of continuous-scale and discrete-scale radiative transfer in metal foams. Journal of Quantitative Spectroscopy and Radiative Transfer. 2018;212:128-38.
[9] Kumar A, Vicente J, Daurelle J-V, Favennec Y, Rousseau B. A numerical method based on domain decomposition to solve coupled conduction-radiation physics using parallel computing within large porous media. Journal of Physics: Conference Series: IOP Publishing; 2021. p. 012057.
[10] Perraudin DY, Haussener S. Numerical quantification of coupling effects for radiation-conduction heat transfer in participating macroporous media: Investigation of a model geometry. International Journal of Heat and Mass Transfer. 2017;112:387-400.
[11] Vignoles GL. A hybrid random walk method for the simulation of coupled conduction and linearized radiation transfer at local scale in porous media with opaque solid phases. International Journal of Heat and Mass Transfer. 2016;93:707-19.
[12] Caliot C, Blanco S, Coustet C, El-Hafi M, Eymet V, Forest V, et al. Combined conductive-radiative heat transfer analysis in complex geometry using the Monte Carlo method. 2019.
[13] Tseng CC, Swanson AD, Viskanta R, Sikorski RL, Chen MY. Effect of foam properties on radiative properties of open-cell silicon carbide foams. Journal of Quantitative Spectroscopy and Radiative Transfer. 2012;113:1503-7.
[14] Avila-Marin AL, Fernandez-Reche J, Gianella S, Ferrari L, Sanchez-Señoran D. Experimental study of innovative periodic cellular structures as air volumetric absorbers. Renewable Energy. 2022;184:391-404.
[15] Taine J, Bellet F, Leroy V, Iacona E. Generalized radiative transfer equation for porous medium upscaling: Application to the radiative Fourier law. International Journal of Heat and Mass Transfer. 2010;53:4071-81.
[16] Guévelou S, Rousseau B, Domingues G, Vicente J, Caliot C. Representative elementary volumes required to characterize the normal spectral emittance of silicon carbide foams used as volumetric solar absorbers. International Journal of Heat and Mass Transfer. 2016;93:118-29.
[17] Tancrez M, Taine J. Direct identification of absorption and scattering coefficients and phase function of a porous medium by a Monte Carlo technique. International Journal of Heat and Mass Transfer. 2004;47:373-83.
[18] Guevelou S, Rousseau B, Domingues G, Vicente J, Caliot C, Flamant G. Evolution of the homogenized volumetric radiative properties of a family of α-SiC foams with growing nominal pore diameter. Journal of Porous Media. 2015;18.
[19] Badri MA, Favennec Y, Jolivet P, Rousseau B. Conductive-radiative heat transfer within SiC-based cellular ceramics at high-temperatures: A discrete-scale finite element analysis. Finite Elements in Analysis and Design. 2020;178.
[20] Gomez-Garcia F, Gonzalez-Aguilar J, Tamayo-Pacheco S, Olalde G, Romero M. Numerical analysis of radiation propagation in a multi-layer volumetric solar absorber composed of a stack of square grids. Solar Energy. 2015;121:94-102.
[21] Coquard R, Baillis D, Randrianalisoa J. Homogeneous phase and multi-phase approaches for modeling radiative transfer in foams. International journal of thermal sciences. 2011;50:1648-63.
[22] Viskanta R, Grosh R. Heat transfer by simultaneous conduction and radiation in an absorbing medium. 1962.